Solar and Stellar Multi-scale Activity
Proceedings IAU Symposium No. 400, 2026
S. Vargas-Domínguez & J. C. Buitrago-Casas, eds.
doi:10.1017/S1743921326107340

Solar Spectropolarimetric Inversions applying Deep Learning Techniques

Juan Esteban Agudelo-Ortiz[1], Santiago Vargas-Domínguez[1], Sergiy Shelyag[2] and Juan Sebastián Castellanos-Durán[3]

[1]Universidad Nacional de Colombia, Observatorio Astronómico Nacional, Bogotá, Colombia
email: juagudeloo@unal.edu.co

[2]College of Science and Engineering, Flinders University, Tonsley, SA 5042, Australia

[3]Max-Planck-Institut für Sonnensystemforschung, Justus-von-Liebig-Weg 3, 37077, Göttingen, Germany

Abstract. Machine Learning applications have gained significant interest in the solar physics community for solving previously intractable problems and accelerating computationally demanding tasks that could otherwise require years to complete. This work presents a novel approach for spectropolarimetric inversions using machine learning models, specifically neural networks, trained with classical supervised methodology enhanced by a physical constraint in the loss function based on the WFA approximation. The results show that a weight of w=0.01 for the physical constraint term yields superior performance in some cases compared to unconstrained models when evaluating metrics such as RRMSE and correlation across different atmospheric depths on synthetic test data. When applied to observational data, although the model struggles with thermodynamic and velocity parameters, the magnetic field generation in the line-of-sight—which relates to the WFA constraint—shows improved generalization when the constraint is applied. These results suggest a promising new approach for developing supervised machine learning models that incorporate physical constraints, guiding them toward a deeper "understanding" of the underlying physics in the analyzed phenomena.

Keywords. Solar, Spectropolarimetry, Photosphere, Neural Networks

1. Introduction

Spectropolarimetric inversions are a fundamental tool for studying the solar atmosphere by analyzing the light we observe from the sun. This light is characterized by its raw intensity and the polarization states that are all described by the so-called Stokes parameters I, Q, U, and V. By means of spectropolarimetric analysis, we can decode the fingerprints encoded by the physical behavior of the solar atmosphere in the emitted light (del Toro Iniesta and Ruiz Cobo 2016). There are various techniques for performing spectropolarimetry, but all of them are based on the same concept of inversion of the Radiative Transfer Equation (RTE), which is the general model that describes how light interacts with a medium (del Toro Iniesta and Ruiz Cobo 2016; del Toro Iniesta 2007; Chandrasekhar 1960). Diverse algorithms have been developed to solve the inversion problem, ranging from numerical methods that assume local thermodynamic equilibrium (LTE) to non-local thermodynamic equilibrium (NLTE) (del Toro Iniesta and Ruiz Cobo 2016). Since these methods tend to be too computationally demanding, in addition to having unrealistic processing times for scientific development, new techniques involving technologies such as Machine Learning models have been developed (Mistryukova et al. 2023; Asensio Ramos et al. 2023a).

© The Author(s), 2026. Published by Cambridge University Press on behalf of The International Astronomical Union. This is an Open Access article, distributed under the terms of the Creative Commons Attribution licence (https://creativecommons.org/licenses/by/4.0/), which permits unrestricted re-use, distribution and reproduction, provided the original article is properly cited.

https://doi.org/10.1017/S1743921326107340 Published online by Cambridge University Press

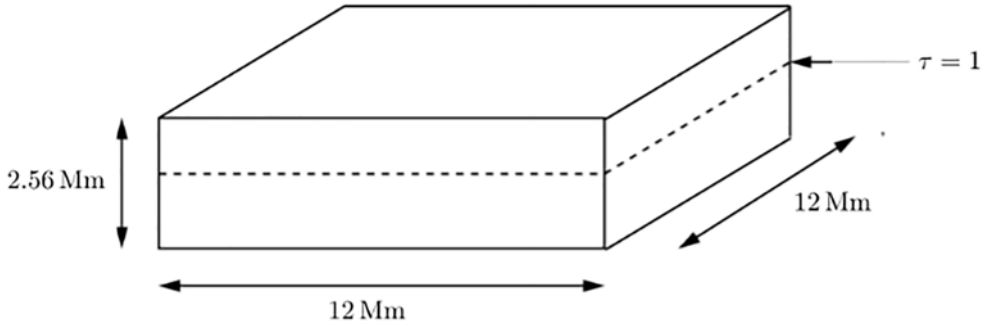


Figure 1. Domain of the MURaM simulated parameters. The domain includes the corrugated surface where the optical depth, τ, meets the condition $\log \tau = 1$, meaning that the domain includes both convective zone and photosphere from the solar atmosphere. The geometrical dimensions of the box are 12 Mm × 12 Mm with a height of 2.56 Mm.

Recent advances in artificial intelligence and machine learning technology have not left the solar physics community indifferent. Various kinds of applications of Machine Learning algorithms have been implemented in recent years, including superresolution models, forecasting algorithms, classification of features in the solar atmosphere at different heights, and segmentation, among others Asensio Ramos et al. (2023b). For the topic that concerns this work, Machine learning algorithms have also been applied for spectropolarimetric inversions. These algorithms vary from simple, deeply connected neural networks that are used for generation or classification, such as the first ever published work on deep learning inversions from Carroll and Staude (2001), to different models that apply convolutions (Asensio Ramos and Díaz Baso 2019; Milić and Gafeira 2020; Gafeira et al. 2021), invertible models (Osborne et al. 2019), and even the application of uncertainty generation (Higgins et al. 2021; Mistryukova et al. 2023).

Continuing this approach, this work aims to create a one dimensional model that is trained on synthetic data using a modified loss function that includes a physical constraint for the magnetic field in the line-of-sight, and then verify its application on actual observations to check its capacity for generalization.

2. Data

2.1. *Model training*

For training the neural network, synthetic data for temperature, T, density, ρ, and both velocity and magnetic field in the line-of-sight (LOS), $v_{\rm LOS}$ and $B_{\rm LOS}$, were generated using the MURaM simulation code Vögler et al. (2005) in a domain that includes both the convective zone and the photosphere, as seen in Fig. 1. In this domain, the atmospheric parameters were generated along geometric height. However, since actual inversion methodologies generate the corresponding atmospheric parameters using optical depth as a measurement of height, it is necessary to perform a mapping from geometrical height to optical depth. This process is applied by using the Rosseland opacities Rose (2001), obtaining 21 optical depth values ranging from $\log \tau = -2.0$ to $\log \tau = 0$ with a sampling of $\log \tau = 0.1$. Apart from the atmospheric parameters, we also have the corresponding spectropolarimetric profiles for each Stokes parameter I, Q, U, and V, which were generated by applying the NLTE numerical code NICOLE (Socas-Navarro et al. 2015) for 300 wavelength points from 6300.5 Å to 6303.5 Å with a spectral sampling of $\Delta\lambda = 0.01$ Å, including the FeI absorption lines in 6301.5 Å and 6302.5 Å. This data was adapted to the Hinode SOT/SP instrument specifications (Tsuneta et al. 2008) by applying the spectral and spatial sampling, the spectral and spatial PSF, and the noise of the

https://doi.org/10.1017/S1743921326107340 Published online by Cambridge University Press

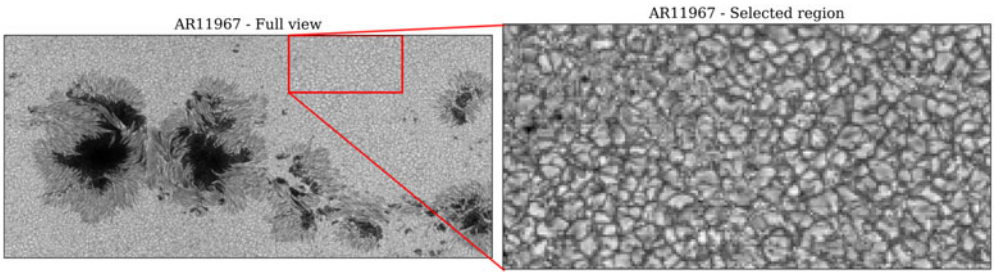


Figure 2. Observation with ID 0560 from the MODEST catalog along with the selected region used for testing the neural network model.

instrument, corresponding to gaussian random noise with a $\sigma = 5 \times 10^{-3}$ of the continuum intensity I_c. Additionally, a weighting was applied to the stokes parameters, realizing that there are differences of orders of magnitude (Lagg et al. 2016; Castellanos Durán et al. 2024) between them, which could lead the neural network to prioritize those with higher magnitudes if not treated properly. Also, We applied a filtering technique using the Otsu threshold (Otsu 1979) to separate both regions with high and low intensity, as well as the regions with high and low polarization This approach allows us to have an equal amount of data from both regions, despite their physically different behaviors (Vögler et al. 2005).

The data extracted correspond to various simulation steps of the MURaM simulation for the quiet sun as observed in the center of the disk. After applying all the preprocessing, we obtained a total of 140 382 pixels for training. For testing the model on synthetic data, a step of the simulation was left outside the training set.

2.2. *Observational*

To test the ability of generalization of the neural network model, it is intended to apply it to actual observations. In this case, an observation corresponding to the MODEST catalog (Castellanos Durán et al. 2024), with ID 0560, was chosen for testing. This observation corresponds to Active region number 11967 from the NOAA Active Region catalog, observed on February 3, 2014, with a field of view of $254'' \times 124''$, longitude $x_c = 16''$, latitude $y_c'' = 126$, and heliocentric angle $\mu = 0.99$, indicating that we are close to the center of the disk. Additionally, based on this observation, we selected a region that did not include the umbra or penumbra. An image on the continuum of this AR, along with the selected region, is shown in Fig. 2. The atmospheric parameters of this observation in the MODEST catalog correspond to SPINOR 2D spatially coupled inversions (Siu-Tapia et al. 2017).

3. Neural Network model

3.1. *Architecture*

Since the data we are dealing with correspond to spectropolarimetric profiles, it is necessary to use a model that can extract as many features as possible from a 1D signal. For this purpose, we used a mixture of convolutional neural networks (CNNs) with deeply connected layers in an architecture named Multi-Scale Convolutional Neural Network (MSCNN; see Fig. 3), which was first implemented by Jiang et al. (2019) with the aim of diagnosing turbine gearbox health through the analysis of the turbine time series. This architecture implements a coarse-grain layer that separates the profiles in different scalings through the application of an average kernel. Each scale passes through a convolutional block that extracts a 1D feature map. All the feature maps are concatenated and

https://doi.org/10.1017/S1743921326107340 Published online by Cambridge University Press

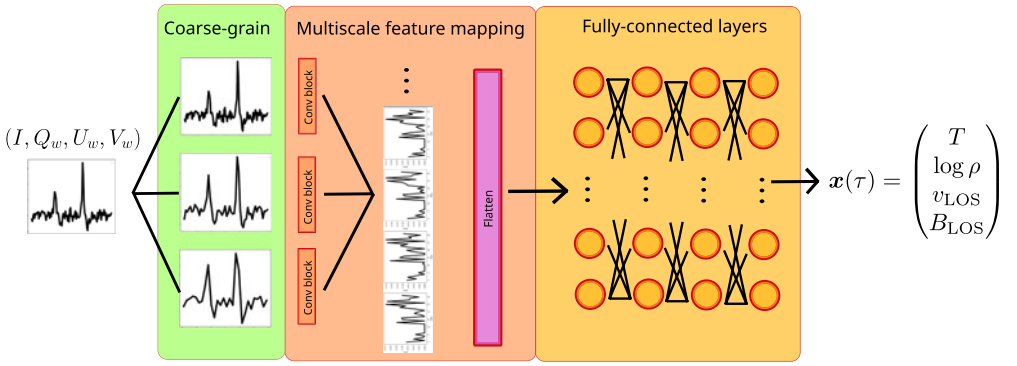


Figure 3. Scheme of the MSCNN architecture. The model receives the weighted stokes parameters, coarse-grain and generate feature maps for each scale for finally passing the concatenated maps to a fully connected neural network block that leads to the output of the corresponding atmospheric parameters.

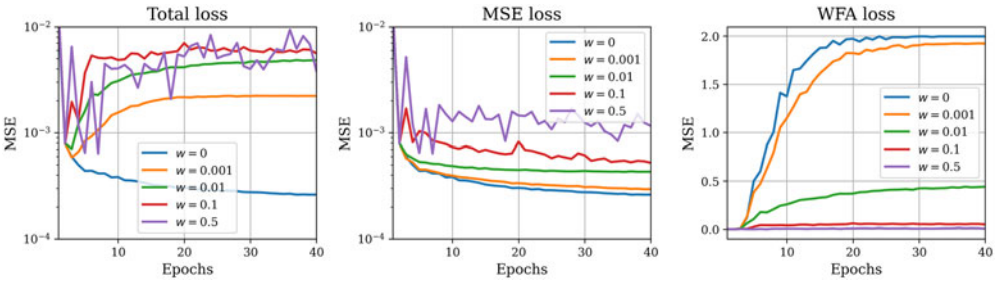


Figure 4. Loss curves for each of the values of the weight w that were used. The left hand figure shows the total loss used for applying the backpropagation over the neural network, while the middle and right hand figures correspond to the MSE loss term and WFA loss term, respectively.

then provided to a fully connected block that retrieves the corresponding atmospheric parameters for each analyzed pixel in its outer layer.

For training the neural network, an Adam optimizer was used, along with a learning rate of 10^{-3} and 40 epochs of training.

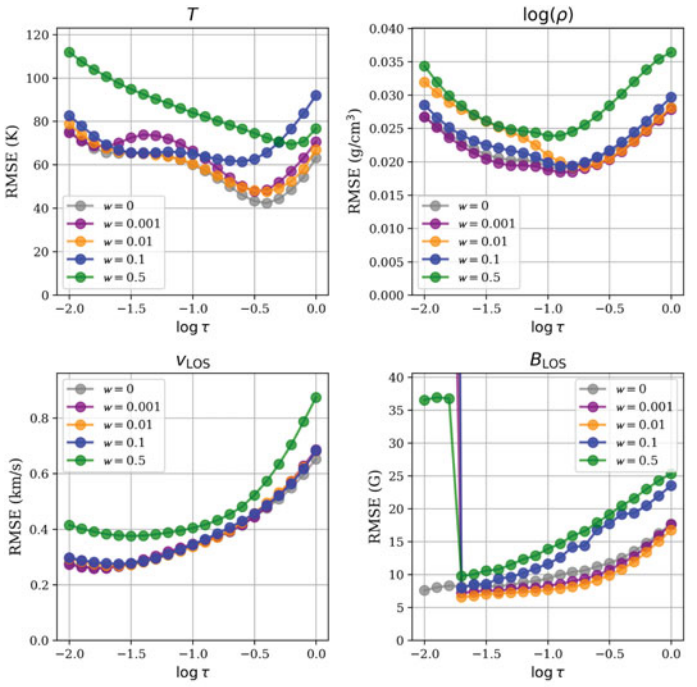
3.2. *Physical constraint*

Based on the idea of Physics-Informed Neural Networks (PINNs; Raissi et al. (2019), we modified the loss function to include a term based on the Weak Field Approximation (WFA) for the $B_{\rm LOS}$. The total loss function uses a weight w to leverage the influence of the terms, where the WFA term is multiplied by w while the mean absolute error (MSE) term is multiplied by $1 - w$). The WFA constraint term compares the magnitude approximation for the magnetic field in the line-of-sight with specific optical depth layers that present the most similarity to the results of the $B_{\rm LOS}$ obtained by the WFA. The approximation is only applied under a threshold of WFA $B_{\rm LOS}$ under 1000 G and also after the MSE loss term reaches values below 4×10^{-4}. The values of w used for the experiment were $w = 0, 0.001, 0.01, 0.1, 0.5$.

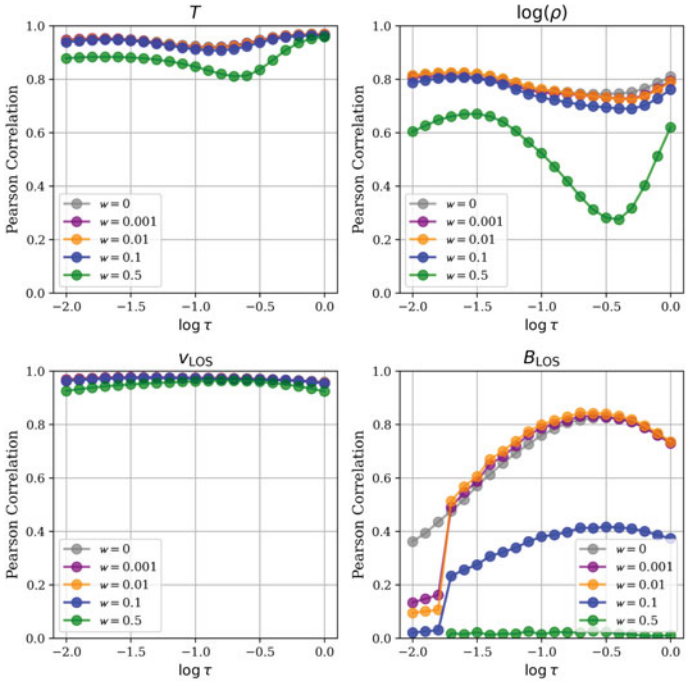
4. Results

The loss curves for the training process of each of the neural networks for each value of the weight w are shown in Fig. 4. As shown by the curves, the most effective behavior

https://doi.org/10.1017/S1743921326107340 Published online by Cambridge University Press



(a) RMSE.



(b) Correlation.

Figure 5. RMSE and correlation values calculated along all optical depth nodes comparing the ground-truth MURaM data with the generated one by the neural netwrok after receiving the corresponding stokes profiles for each pixel.

https://doi.org/10.1017/S1743921326107340 Published online by Cambridge University Press

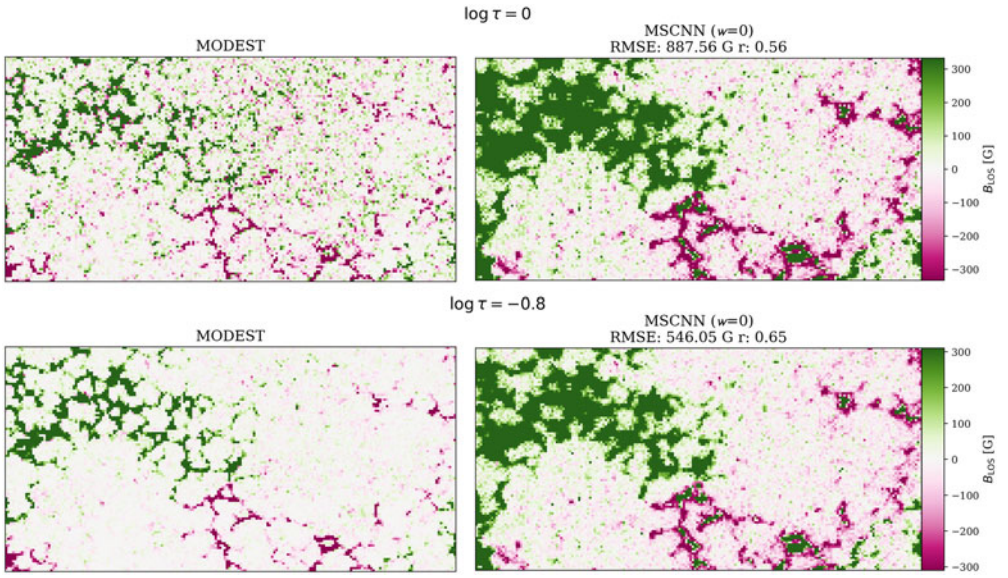


Figure 6. Comparison between the magnetic field in the line-of-sight from the MODEST nodes $\log \tau = -0.8, 0$ with the one generated with the MSCNN model with not constraint applied in the loss function.

curve that balances the influence of both the typical MSE loss and the WFA term corresponds to the curve of $w = 0.01$, which could indicate that the resulting model with this weight value would find a better equilibrium between data information and the physical information of the magnetic field.

The RMSE and correlation values calculated along the optical depth for the MURaM test set compared to the generated data using the MSCNN model are shown in Fig. 5. From these plots, one could infer that, in general, the best RMSE and correlation values along optical depth would correspond to $w = 0, 0.01$, whereas, in some cases, $w = 0.01$ seems to outperform the results with no constraint.

When applied to the observations from the MODEST catalog, Fig. 6 and Fig. 7 show a comparison between the resulting quantities for both weights $w = 0, 0.01$. As can be seen, the MSCNN model with the physical constraint presents results of sharper magnetic fields compared to those of the case without constraint; however, it introduces confusion regarding the direction of the magnetic field flux. Additionally, the RMSE value decreases when the constraint is applied, indicating that the constraint allows for better generalization of the machine learning model when applied to observational data compared to state-of-the-art numerical methods. We only show the resulting magnetic field in the LOS since the thermodynamic quantities and $v_{\rm LOS}$ differ greatly from what is obtained by SPINOR 2D in all cases.

5. Discussion

According to the results of the model applíed to the synthetic data for testing, it appears that the model is capable of replicating the atmospheric parameters with remarkable precision and even improving the generation when the WFA constraint is applied. This result replicates when applied to the observational data for the case of the magnetic field in the line-of-sight, noting that when applying the physical constraint, the physical generation of the results compared to those obtained from SPINOR 2D improves.

https://doi.org/10.1017/S1743921326107340 Published online by Cambridge University Press

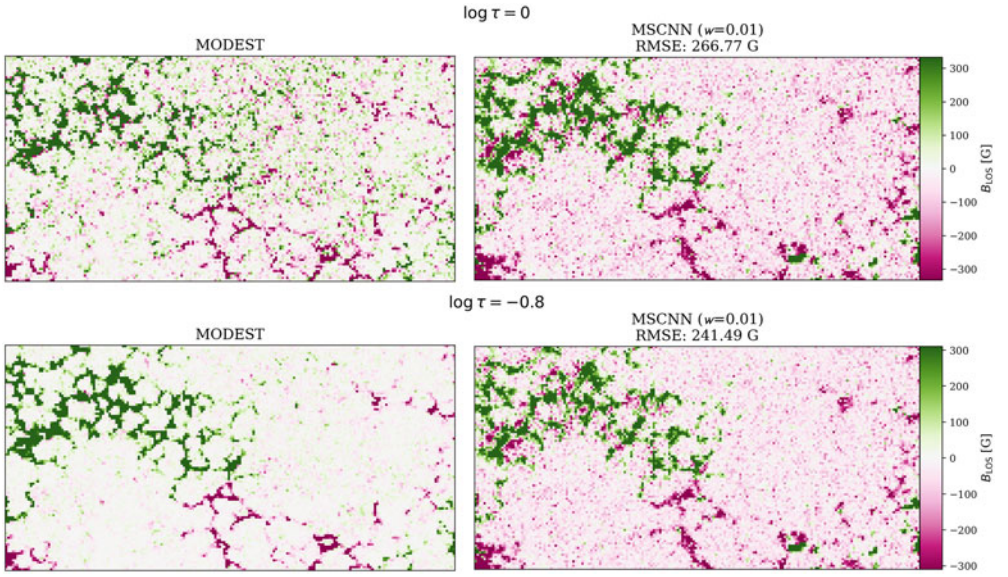


Figure 7. Comparison between the magnetic field in the line-of-sight from the MODEST nodes $\log \tau = -0.8, 0$ with the one generated with the MSCNN model with the constraint applied on the loss function with $w = 0.01$

However, it is important to mention that for the remaining parameters, the generalization was not as good, probably indicating that the addition of other constraints is needed.

In general, this work, which is the first in its class on implementing physical constraints based on approximations of the radiative transfer inversion problem as a constraint for applying spectropolarimetric inversions, shows promising results that could motivate the application of physical constraints on data driven models for refining their generalization capabilities. These could also provide hints that an interesting approach for applying machine learning algorithms to analyze solar phenomena might involve supplying information about the physical behavior of the system we are studying to the model in order to achieve improved accuracy.

References

Asensio Ramos, A., Cheung, M. C. M., Chifu, I., and Gafeira, R. (2023a). Machine learning in solar physics. *Living Reviews in Solar Physics*, 20(1):4.

Asensio Ramos, A., Cheung, M. C. M., Chifu, I., and Gafeira, R. (2023b). Machine learning in solar physics. *Living Reviews in Solar Physics*, 20(1):4.

Asensio Ramos, A. and Díaz Baso, C. J. (2019). Stokes inversion based on convolutional neural networks. *A&A*, 626:A102.

Carroll, T. A. and Staude, J. (2001). The inversion of Stokes profiles with artificial neural networks. *A&A*, 378:316–326.

Castellanos Durán, J. S., Milanovic, N., Korpi-Lagg, A., Löptien, B., van Noort, M., and Solanki, S. K. (2024). The modest catalog of depth-dependent spatially coupled inversions of sunspots observed by hinode/sot-sp. *Astronomy & Astrophysics*, 687:A218.

Chandrasekhar, S. (1960). *Radiative transfer*.

del Toro Iniesta, J. C. (2007). *Introduction to Spectropolarimetry*.

del Toro Iniesta, J. C. and Ruiz Cobo, B. (2016). Inversion of the radiative transfer equation for polarized light. *Living Reviews in Solar Physics*, 13(1):4.

Gafeira, R., Orozco Suárez, D., Milić, I., Quintero Noda, C., Ruiz Cobo, B., and Uitenbroek, H. (2021). Machine learning initialization to accelerate Stokes profile inversions. *A&A*, 651:A31.

https://doi.org/10.1017/S1743921326107340 Published online by Cambridge University Press

Higgins, R. E. L., Fouhey, D. F., Zhang, D., Antiochos, S. K., Barnes, G., Hoeksema, J. T., Leka, K. D., Liu, Y., Schuck, P. W., and Gombosi, T. I. (2021). Fast and Accurate Emulation of the SDO/HMI Stokes Inversion with Uncertainty Quantification. *ApJ*, 911(2):130.

Jiang, G., He, H., Yan, J., and Xie, P. (2019). Multiscale Convolutional Neural Networks for Fault Diagnosis of Wind Turbine Gearbox. *IEEE Transactions on Industrial Electronics*, 66(4):3196–3207.

Lagg, A., Solanki, S. K., Doerr, H. P., Martínez González, M. J., Riethmüller, T., Collados Vera, M., Schlichenmaier, R., Orozco Suárez, D., Franz, M., Feller, A., Kuckein, C., Schmidt, W., Asensio Ramos, A., Pastor Yabar, A., von der Lühe, O., Denker, C., Balthasar, H., Volkmer, R., Staude, J., Hofmann, A., Strassmeier, K., Kneer, F., Waldmann, T., Borrero, J. M., Sobotka, M., Verma, M., Louis, R. E., Rezaei, R., Soltau, D., Berkefeld, T., Sigwarth, M., Schmidt, D., Kiess, C., and Nicklas, H. (2016). Probing deep photospheric layers of the quiet Sun with high magnetic sensitivity. *A&A*, 596:A6.

Milić, I. and Gafeira, R. (2020). Mimicking spectropolarimetric inversions using convolutional neural networks. *A&A*, 644:A129.

Mistryukova, L., Plotnikov, A., Khizhik, A., Knyazeva, I., Hushchyn, M., and Derkach, D. (2023). Stokes inversion techniques with neural networks: analysis of uncertainty in parameter estimation. *Solar Physics*, 298(8):98.

Osborne, C. M. J., Armstrong, J. A., and Fletcher, L. (2019). RADYNVERSION: Learning to Invert a Solar Flare Atmosphere with Invertible Neural Networks. *ApJ*, 873(2):128.

Otsu, N. (1979). A Threshold Selection Method from Gray-Level Histograms. *IEEE Transactions on Systems, Man, and Cybernetics*, 9(1):62–66.

Raissi, M., Perdikaris, P., and Karniadakis, G. (2019). Physics-informed neural networks: A deep learning framework for solving forward and inverse problems involving nonlinear partial differential equations. *Journal of Computational Physics*, 378:686–707.

Rose, S. J. (2001). The radiative opacity at the Sun centre-a code comparison study. *J. Quant. Spec. Radiat. Transf.*, 71:635–638.

Siu-Tapia, A., Lagg, A., Solanki, S. K., van Noort, M., and Jurčák, J. (2017). Normal and counter Evershed flows in the photospheric penumbra of a sunspot. SPINOR 2D inversions of Hinode-SOT/SP observations. *A&A*, 607:A36.

Socas-Navarro, H., de la Cruz Rodríguez, J., Asensio Ramos, A., Trujillo Bueno, J., and Ruiz Cobo, B. (2015). An open-source, massively parallel code for non-LTE synthesis and inversion of spectral lines and Zeeman-induced Stokes profiles. *A&A*, 577:A7.

Tsuneta, S., Ichimoto, K., Katsukawa, Y., Nagata, S., Otsubo, M., Shimizu, T., Suematsu, Y., Nakagiri, M., Noguchi, M., Tarbell, T., Title, A., Shine, R., Rosenberg, W., Hoffmann, C., Jurcevich, B., Kushner, G., Levay, M., Lites, B., Elmore, D., Matsushita, T., Kawaguchi, N., Saito, H., Mikami, I., Hill, L. D., and Owens, J. K. (2008). The Solar Optical Telescope for the Hinode Mission: An Overview. *Sol. Phys.*, 249(2):167–196.

Vögler, A., Shelyag, S., Schüssler, M., Cattaneo, F., Emonet, T., and Linde, T. (2005). Simulations of magneto-convection in the solar photosphere. Equations, methods, and results of the MURaM code. *A&A*, 429:335–351.

https://doi.org/10.1017/S1743921326107340 Published online by Cambridge University Press